DISSERTATIONS IN
FORESTRY AND
NATURAL SCIENCES

Ismo Vartiainen

Polarization control and coherence–polarization mixing by sub-wave-length gratings

Publications of the University of Eastern Finland
Dissertations in Forestry and Natural Sciences

UNIVERSITY OF
EASTERN FINLAND

ISMO VARTIAINEN

Polarization control and coherence–polarization mixing by sub-wavelength gratings

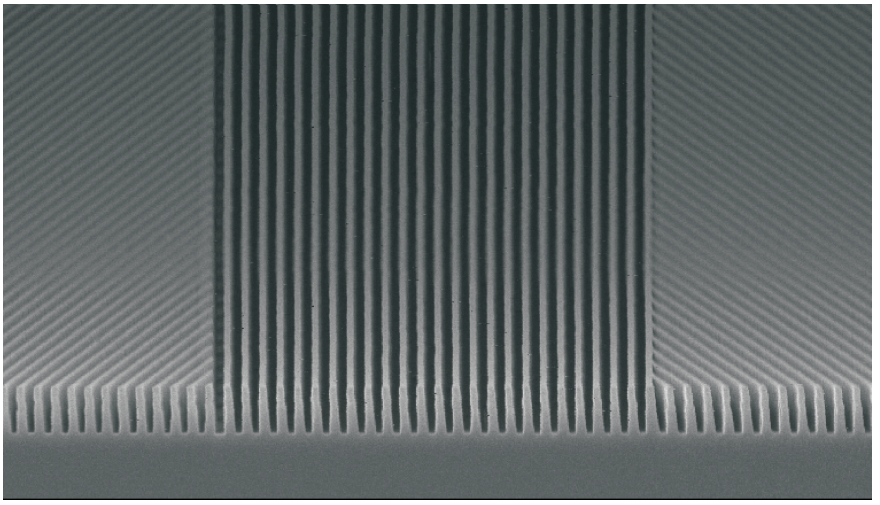

Publications of the University of Eastern Finland
Dissertations in Forestry and Natural Sciences
No 58

Academic Dissertation
To be presented by permission of the Faculty of Science and Forestry for public examination in the Auditorium M100 in Metria Building at the University of Eastern Finland, Joensuu, on December, 16, 2011,
at 12 o'clock noon.

Department of Physics and Mathematics

Kopijyvä Oy
Joensuu, 2011
Editor: Prof. Pertti Pasanen
Prof. Kai Peiponen, Prof. Matti Vornanen

Distribution:
University of Eastern Finland Library / Sales of publications
P.O. Box 107, FI-80101 Joensuu, Finland
tel. +358-50-3058396
http://www.uef.fi/kirjasto

ISBN: 978-952-61-0619-9 (printed)
ISSNL: 1798-5668
ISSN: 1798-5668
ISBN: 978-952-61-0620-5 (pdf)
ISSNL: 1798-5668
ISSN: 1798-5676

Author's address:
University of Eastern Finland
Department of Physics and Mathematics
P.O.Box 111
80101 Joensuu
FINLAND
email: ismo.vartiainen@uef.fi

Supervisors:
Professor Markku Kuittinen, Ph.D.
Department of Physics and Mathematics
P.O.Box 111
80101 Joensuu
FINLAND
email: markku.kuittinen@uef.fi

Jani Tervo, Ph.D., Docent
Department of Physics and Mathematics
P.O.Box 111
80101 Joensuu
FINLAND
email: jani.tervo@uef.fi

Toni Saastamoinen, Ph.D.
Department of Physics and Mathematics
P.O.Box 111
80101 Joensuu
FINLAND
email: toni.saastamoinen@uef.fi

Reviewers:
Uwe D. Zeitner, Dr.
Fraunhofer Institute for Applied Optics and Precision Engineering
A.-Einstein-Str. 7
07745 Jena
GERMANY
email: uwe.zeitner@iof.fraunhofer.de

Tero Setälä, D.Sc. (Tech.)
Aalto University
Department of Applied Physics
P.O. Box 13500
FI-00076 Aalto
FINLAND
email: tero.setala@tkk.fi

Opponent:
Professor Massimo Santarsiero, Ph.D.
Universita Roma Tre and CNISM
Dipartimento di Fisica
via della Vasca Navale, 84
00146 Rome
ITALY
email: santarsiero@fis.uniroma3.it

ABSTRACT

This thesis is a survey of polarization control by means of sub-wavelength gratings. The thesis begins with a brief theoretical summary of the fields of electromagnetic theory, coherence theory, and polarization. The thesis considers inverse polarization effect in surface-relief gratings, where the function of the structures is based on grating anomalies, in contrast to classical polarization control devices. The design of the aforementioned structures using rigorous methods as well as fabrication by electron beam lithography is discussed. Furthermore, experimental results for polarization gratings for lossless beam splitting and for measurement of Stokes parameters are described. In addition, this thesis gives insight for new optical phenomenon called coherence-polarization mixing, in which partial correlation of the polarization components is transferred to partial polarization.

Universal Decimal Classification: 535.42, 535.51, 681.7.063
PACS Classification: 07.60.-j, 42.25.Fx, 42.25.Ja, 42.25.Kb, 42.79.Dj, 42.79.Gn, 81.07.-b, 81.16.Nd
INSPEC Thesaurus: optics; micro-optics; optical elements; optical fabrication; nanotechnology; electron beam lithography; etching; metals; polarisation; resonance; surface plasmons; optical filters; optical waveguides; diffraction gratings; light coherence; electromagnetic theory of light
Yleinen suomalainen asiasanasto: optiikka; optiset laitteet; optiset hilat; valmistustekniikka; mikrotekniikka; nanotekniikka; litografia; etsaus; metallit; polarisaatio; resonanssi; diffraktio; koherenssi

Preface

First of all I would like to express my deepest gratitude to my supervisors Prof. Markku Kuittinen, Jani Tervo, and Toni Saastamoinen. I was privileged to start working in the group even before starting my PhD studies in the supervision of Prof. Kuittinen and from then on this work has been fruitful and hopefully it shall continue like that. Jani has been a source of wonderful ideas that I have been trying to establish with my best effort. Toni has offered his help in technical issues whenever I have needed. I would also like to thank the former head of department of Physics and Mathematics Prof. Timo Jääskeläinen and the current one Prof. Pasi Vahimaa for the opportunity to work in our department.

I am extremely grateful for all the past and current co-workers. Without them, our wonderful team spirit could have never been achieved, which is essential for our creative field of work.

The reviewers Dr Tero Setälä and Dr Uwe Zeitner are highly acknowledged for their statements and comments that helped me to improve the thesis. In addition, I am grateful for the personal grants from Emil Aaltonen Foundation and Finnish Foundation of Technology.

Finally, I would like to thank my mother and father for their help and support during all these years. And last but not least, I would like to thank Jenni for her encouragement and trust whenever I needed it the most.

Joensuu November 25, 2011 *Ismo Vartiainen*

LIST OF PUBLICATIONS

This thesis consists of the present review of the author's work in the field of photonics and the following selection of the author's publications:

I I. Vartiainen, J. Tervo, and M. Kuittinen, "Depolarization of quasi-monochromatic light by thin resonant gratings," *Opt. Lett.* **34,** 1648–1650 (2009).

II I. Vartiainen, J. Tervo, J. Turunen, and M. Kuittinen, "Surface-relief polarization gratings for visible light," *Opt. Express* **18,** 22850–22858 (2010).

III A. Lehmuskero, I. Vartiainen, T. Saastamoinen, T. Alasaarela, and M. Kuittinen, "Absorbing polarization selective resonant gratings," *Opt. Express* **18,** 27270–27279 (2010).

IV G. Kang, I. Vartiainen, B. Bai, H. Tuovinen, and J. Turunen, "Inverse polarizing effect of subwavelength metallic gratings in deep ultraviolet band," *Appl. Phys. Lett.* **99,** 071103 (2011).

V I. Vartiainen, T. Saastamoinen, J. Tervo, and M. Kuittinen, "Coherence–polarization mixing in resonance gratings," submitted to *Opt. Lett.* (2011).

Throughout the overview, these papers will be referred to by Roman numerals. In addition, studies on micro- and nano-optics and optical measurements have been published in articles [1–11] in which the author has been a co-author.

AUTHOR'S CONTRIBUTION

The publications selected in this dissertation are original research papers on polarization control and coherence–polarization mixing by sub-wavelength gratings.

In papers **I**, **II**, **IV**, and **V** the author has made all the designs of the structures, and performed the fabrication and the optical measurements of the elements in papers **II** and **IV**. In addition, the author has written most of the manuscript in papers **I**, **II**, and **V** and has participated in writing of the experimental part of the paper **IV**.

The author has conducted the fabrication of the grating in paper **III** and has written the fabrication part of that manuscript. In all papers the co-operation with the co-authors has been significant.

Contents

1 Introduction

Light has a dualistic nature, known as wave-particle duality, in which some of the phenomena in light and matter interaction can be explained by the wave nature and some by particle nature of light. With the findings of Isaac Newton [12] and Thomas Young [13] and many before them, these theories seemed to be separated. Later on, theories supporting the wave nature were unified to the theory of electromagnetism by James Clerk Maxwell [14]. On the other side of the puzzle, Albert Einstein improved the work of his antecessors and was able to explain some of the physical difficulties of that time. Light particle was named the photon. Coexistence of both of the theories was understood as mandatory to explain all the phenomena related to light, and these theories are still routinely used to model the light and matter interactions.

Shaping light and harnessing its potential has fascinated humankind for centuries. This has been motivated by the interest in the structure of the galaxy and distant planets in the sky as well as microscopic structures in living cells. Both of these aspects require the understanding of the nature of light and innovative ways of controlling it.

Nature is full of remarkable examples on innovative means of exploiting light. Human eye, for example, with its complex structure can easily be considered as one the most adaptive and effective detectors for visible light. Man have wisely tapped the products of nature's repetitious development of optical components, thus the evolution has done the optimization for us. Development of light sources [15, 16] and fabrication methods [17–19] of optical micro- and nanostructures together with improved theoretical knowledge [20] has led to a current situation where artificial optical components and light sources are found everywhere.

Invention of laser [21–23] was probably the most important discovery in optics during the last century and brought recognition

to the laser pioneers Charles Hard Townes, Nikolai G. Basov, and Alexander M. Prokhorov in 1964 and to Alfred Kastler [24] in 1966 in the form of Nobel prizes in Physics. Invention of laser further provoked the development of optical coherence theory that was earlier a minor field of research. Some of the famous researchers before the time of lasers should be mentioned, such as P. H. Van Cittert and Frits Zernike [25], who evoked the field in 1930s. The most profound studies, that still are frequently referred to, were presented by Leonard Mandel and Emil Wolf. "Little did we know how rapidly the subject would develop and that it would become a cornerstone of an essentially new field, now known as quantum optics", stated Mandel and Wolf in the preface of the book *Optical Coherence and Quantum Optics* in 1995 [26]. Nowadays the topic attracts more attention due to the applications fueled by the laser sources such as display technologies [27,28], radar systems [29,30], and many others.

This thesis focuses on the control and manipulation of polarization properties of light by structures with sub-wavelength features. We show numerical and experimental results for polarization division by exploiting optical resonances. In addition, we demonstrate experimental results for beam splitters exceeding the scalar diffraction efficiency. We present numerical results of interesting topic we call coherence–polarization mixing. The name refers to phenomenon where partial coherence is transferred to partial polarization. Moreover, this thesis presents ways for polarization division utilizing optical resonances and spatial modulation on the polarization of light.

This thesis is organized as follows: Fundamentals of electromagnetic theory as well as optical coherence theory and polarization will be introduced in chapter 2. Chapter 3 describes diffractive optical elements, focusing on two important topics of this thesis, namely guided mode resonance gratings and polarization division structures. Their physical properties as well as applications are discussed. Fabrication techniques of these structures are presented in chapter 4, concentrating on the methods used in this thesis. The

main results of this thesis are illustrated in chapter 5, giving future prospects on the topics. The work is concluded in chapter 6.

2 Fundamentals of electromagnetic theory

Thomas Young discovered the wave nature of light in the beginning of the 19th century by observing the local intensity variations of light behind two narrow slits [13]. Later Maxwell integrated the work of Coulomb, Ampere, Örsted, Faraday, and many others to the theory of electromagnetism [14]. Emil Wolf can be considered as a pioneer in the coherence theory, especially in scalar domain [26]. His findings are still used routinely for characterizing partially coherent fields. The growing need of tools for analyzing vectorial partially coherent fields has provoked the research on this field recently [31–38].

In this chapter, we cover the main theory for modeling electromagnetic fields. Moreover, we define the polarization by means of Jones calculus and recall the principles of coherence theory.

2.1 COMPLEX ANALYTIC SIGNAL

All the basic quantities of optical fields should be measurable and therefore real-valued functions of space and time. However, it is more convenient to represent the field in the complex form [26, 39]. This makes the mathematics more straightforward, since we are not forced to deal with trigonometric functions. Let us assume a real valued field $\mathbf{U}_\mathrm{r}$ with real variables $\mathbf{r}$ and t. Assuming that the field is square-integrable, it can be expressed as a Fourier integral of the monochromatic fields in the form

$$\mathbf{U}_\mathrm{r}(\mathbf{r},t) = \int_{-\infty}^{\infty} \tilde{\mathbf{U}}_\mathrm{r}(\mathbf{r},\omega)\exp(-\mathrm{i}\omega t)\,\mathrm{d}\omega, \tag{2.1}$$

where

$$\tilde{\mathbf{U}}_\mathrm{r}(\mathbf{r},\omega) = \frac{1}{2\pi}\int_{-\infty}^{\infty} \mathbf{U}_\mathrm{r}(\mathbf{r},t)\exp(\mathrm{i}\omega t)\,\mathrm{d}t, \tag{2.2}$$

and $\mathbf{r}$ is position vector, ω is angular frequency, t is time and i is the imaginary unit. Since $\mathbf{U}_\mathrm{r}$ is real, $\tilde{\mathbf{U}}_\mathrm{r}$ must be Hermitian, so that $\tilde{\mathbf{U}}_\mathrm{r}(r,-\omega) = \tilde{\mathbf{U}}_\mathrm{r}^*(r,\omega)$, where $*$ denotes complex conjugate. Hence, the negative frequencies do not carry any information that is not covered in the positive frequencies, therefore we may define a new function

$$\mathbf{U}(\mathbf{r},t) = 2\int_0^\infty \tilde{\mathbf{U}}_\mathrm{r}(\mathbf{r},\omega)\exp(-\mathrm{i}\omega t)\,\mathrm{d}\omega, \tag{2.3}$$

that is called the complex analytic signal [39], which is associated to the real function,

$$\mathbf{U}_\mathrm{r}(\mathbf{r},t) = \Re\{\mathbf{U}(\mathbf{r},t)\}. \tag{2.4}$$

The complex analytic signal may also be expressed as a Fourier transform

$$\mathbf{U}(\mathbf{r},t) = \int_{-\infty}^\infty \tilde{\mathbf{U}}(\mathbf{r},\omega)\exp(-\mathrm{i}\omega t)\,\mathrm{d}\omega, \tag{2.5}$$

where

$$\tilde{\mathbf{U}}(\mathbf{r},\omega) = \frac{1}{2\pi}\int_{-\infty}^\infty \mathbf{U}(\mathbf{r},t)\exp(\mathrm{i}\omega t)\,\mathrm{d}t. \tag{2.6}$$

The complex and the real spectra are now related to each other by

$$\tilde{\mathbf{U}}(\mathbf{r},\omega) = \begin{cases} 2\tilde{\mathbf{U}}_\mathrm{r}(\mathbf{r},\omega), & \text{when} \quad \omega \geq 0 \\ 0, & \text{when} \quad \omega < 0 \end{cases}. \tag{2.7}$$

Analogous expressions hold for all the electromagnetic field components. Throughout this thesis we use the complex analytic signal for presenting electromagnetic field.

2.2 COHERENCE THEORY

To simplify the analysis, the electromagnetic fields are often modeled as fully coherent. However, this is not rigorously true for any naturally generated field, as the variation of phase and also intensity may be random in time or space. In this section, the theory for modeling such random processes will be discussed as we recall the principles of the optical coherence theory.

2.2.1 Expectation value of a random process

Let us consider a random function, say some field component $U(t)$, that fluctuates in time and has a probability density $p(U,t)$, that denotes the probability for the random function $U(t)$ to take the value U at instant t. For any random process we can calculate the expectation value

$$\langle U(t)\rangle = \int U p(U,t)\mathrm{d}U. \tag{2.8}$$

The set of all realizations U_n is called the statistical ensemble of $U(t)$. Alternatively we may calculate the expectation of U at time t as an average over the ensemble of all the realizations

$$\langle U(t)\rangle = \lim_{N\to\infty}\frac{1}{N}\sum_{n=1}^{N} U_n(t). \tag{2.9}$$

2.2.2 Two-fold autocorrelation function

Above we considered the expectation values of single realizations or ensembles of all the realizations. This gives us no information about the correlation between two instants of time (and space) for the random variables $U(t_1)$ and $U(t_2)$. For this, we may define the joint or two-fold probability density by

$$p[U(t_1);U(t_2)] = p(U_1,t_1;U_2,t_2). \tag{2.10}$$

The correlation of $U(t_1)$ and $U(t_2)$ can be described by two-time autocorrelation function

$$\Gamma(t_1,t_2) = \langle U^*(t_1)U(t_2)\rangle = \iint U_1^* U_2 p(U_1,t_1;U_2,t_2)\,\mathrm{d}U_1\mathrm{d}U_2, \tag{2.11}$$

or alternatively

$$\Gamma(t_1,t_2) = \lim_{N\to\infty}\frac{1}{N}\sum_{n=1}^{N} U_n^*(t_1)U_n(t_2). \tag{2.12}$$

It follows from the definition of Γ that

$$\langle I(t)\rangle = \Gamma(t,t) = \langle |U(t)|^2\rangle, \tag{2.13}$$

where $\langle I(t) \rangle$ is the expectation value of the instantaneous intensity [26].

2.2.3 Complex degree of coherence

Up to this point we have considered the correlation at two instants of time. More generally, one may be interested in the correlations between two separate points in space and time. Moreover, the field may have some variation in time, but the second-order statistical measures like mean value and correlations are time-independent. Fields with such properties are called statistically stationary at least in the wide sense. In this thesis we consider continuous sources that can be treated as statistically stationary. With these assumptions, the mutual coherence matrix takes the form

$$\Gamma(\mathbf{r}_1, \mathbf{r}_2, \tau) = \langle U^*(\mathbf{r}_1, t) U(\mathbf{r}_2, t + \tau) \rangle. \tag{2.14}$$

The normalized form of Γ,

$$\gamma(\mathbf{r}_1, \mathbf{r}_2, \tau) = \frac{\Gamma(\mathbf{r}_1, \mathbf{r}_2, \tau)}{\sqrt{I(\mathbf{r}_1) I(\mathbf{r}_2)}}, \tag{2.15}$$

is called the complex degree of coherence. It follows from the Schwartz inequality that

$$0 \leq |\gamma(\mathbf{r}_1, \mathbf{r}_2, \tau)| \leq 1. \tag{2.16}$$

If $\gamma = 0$ the field is completely uncorrelated at points $\mathbf{r}_1$ and $\mathbf{r}_2$. If $|\gamma| = 1$ for all pairs $\mathbf{r}_1$ and $\mathbf{r}_2$, the field is completely correlated. However, all the naturally generated fields are partially correlated even though the value of $|\gamma|$ may be close to one for some laser sources and nearly zero for some thermal sources [40, 41].

2.2.4 Cross-spectral density

As nearly all of the optical "constants" are frequency-dependent, it is more convenient to examine the correlations in the space–frequency domain rather than in the space–time domain. The mu-

tual coherence function can be related to the space–frequency domain function by a Fourier transform

$$\Gamma(\mathbf{r}_1, \mathbf{r}_2, \tau) = \int_0^\infty W(\mathbf{r}_1, \mathbf{r}_2, \omega) \exp(\mathrm{i}\omega\tau)\mathrm{d}\omega, \tag{2.17}$$

where

$$W(\mathbf{r}_1, \mathbf{r}_2, \omega) = \frac{1}{2\pi} \int_{-\infty}^\infty \Gamma(\mathbf{r}_1, \mathbf{r}_2, \tau) \exp(-\mathrm{i}\omega\tau)\mathrm{d}\tau. \tag{2.18}$$

The function in Eq. (2.18) is called the cross-spectral density function (CSD), and the Fourier transform pair defined in equations (2.17) and (2.18) is known as the generalized Wiener–Khintchine theorem [42–44]. Analogously to the space–time domain intensity, we can define intensity at frequency ω

$$S(\mathbf{r}, \omega) = W(\mathbf{r}, \mathbf{r}, \omega), \tag{2.19}$$

which is called the spectral density.

2.2.5 Partial coherence of scalar fields

When modeling the light interaction with micro- or nanometer scale structures one usually assumes fully coherent illumination due to the complexity of the problem. This is often justified by the use of highly coherent sources such as gas lasers. If one needs to deal with partially coherent illumination, the field needs to be decomposed to fully coherent fields. One solution for this is to use Mercer's theorem, hence the CSD function may be expressed in the form

$$W(\mathbf{r}_1, \mathbf{r}_2, \omega) = \sum_{n=1}^{N} \alpha_n \psi_n^*(\mathbf{r}_1, \omega)\psi_n(\mathbf{r}_2, \omega), \tag{2.20}$$

where α_n and ψ_n are the eigenvalues and eigenfunctions of a homogenous Fredholm's integral equation of the first kind [26]. The eigenfunctions in Eq. (2.20) form an orthonormal set of completely coherent and mutually uncorrelated modes, that fulfill both the Hermiticity and the nonnegative definiteness conditions [26]. The

eigenvalues can be understood to represent the energy distribution of the modes. The expression in Eq. (2.20) can be used in analysis of partially coherent scalar fields. In addition, Wolf showed [45] that the cross-spectral density can be expressed as a correlation function in space–frequency domain: Let $\{U(\mathbf{r},\omega)\exp(-\mathrm{i}\omega t)\}$ represent an ensemble of monochromatic oscillations, where $U(\mathbf{r},\omega)$ is scalar amplitude and t is time. The cross-spectral density can be expressed as [45]

$$W(\mathbf{r}_1,\mathbf{r}_2,\omega) = \langle U^*(\mathbf{r}_1,\omega)U(\mathbf{r}_2,\omega)\rangle, \tag{2.21}$$

where angle brackets denote ensemble averaging. Theory of partially coherent fields described by Wolf is commonly used for analysis of such fields. However, rigorous treatment of vector valued electromagnetic fields needs some expansion of the theory. Next we briefly recall the results for analyzing partially coherent electromagnetic fields by Tervo, *et al.* [34].

2.2.6 Partial coherence of electromagnetic fields

The coherence properties of electromagnetic fields can be expressed using a 3×3 mutual coherence tensor that describes the correlations of electromagnetic field vectors in space-time domain as

$$\boldsymbol{\mathcal{E}}(\mathbf{r}_1,\mathbf{r}_2,\tau) = [\mathcal{E}_{ij}(\mathbf{r}_1,\mathbf{r}_2,\tau)] = \langle \mathbf{E}^\dagger(\mathbf{r}_1,t)\mathbf{E}(\mathbf{r}_2,t+\tau)\rangle, \tag{2.22}$$

where $\dagger$ denotes the Hermitian adjoint, $\mathbf{E}(\mathbf{r},t)$ is a realization of the electric field at point $\mathbf{r}$ at time t, and τ is time difference. The mutual coherence tensor can be shown to be Hermitian, i.e. $\boldsymbol{\mathcal{E}}(\mathbf{r}_2,\mathbf{r}_1,-\tau) = \boldsymbol{\mathcal{E}}^\dagger(\mathbf{r}_1,\mathbf{r}_2,\tau)$ and it fulfills the nonnegative definiteness condition and is square integrable in any finite domain D. Therefore we may define its Fourier transform as

$$\mathcal{W}_{ij}(\mathbf{r}_1,\mathbf{r}_2,\omega) = \frac{1}{2\pi}\int_{-\infty}^{\infty} \mathcal{E}_{ij}(\mathbf{r}_1,\mathbf{r}_2,\tau)\exp(-\mathrm{i}\omega\tau)\,\mathrm{d}\tau, \tag{2.23}$$

where

$$\mathcal{E}_{ij}(\mathbf{r}_1,\mathbf{r}_2,\tau) = \int_0^{\infty} \mathcal{W}_{ij}(\mathbf{r}_1,\mathbf{r}_2,\omega)\exp(\mathrm{i}\omega\tau)\,\mathrm{d}\omega. \tag{2.24}$$

The tensor defined in Eq. (2.23) is called the (electric) cross-spectral density tensor. The lower limit in Eq. (2.24) is zero because the electric field is defined using complex analytic signal representation. In addition, the components of cross-spectral density tensor in Eq. (2.23) are Hermitian, fulfill the nonnegative definiteness conditions, and are square integrable. Moreover, the (electric) cross-spectral density tensor can be expressed as a Mercer-type series of the form

$$\boldsymbol{\mathcal{W}}(\mathbf{r}_1, \mathbf{r}_2, \omega) = \sum_n \lambda_n \boldsymbol{\phi}_n^\dagger(\mathbf{r}_1, \omega) \boldsymbol{\phi}_n(\mathbf{r}_2, \omega), \tag{2.25}$$

where λ_n and $\boldsymbol{\phi}_n$ are the eigenvalues and vector-valued eigenfunctions, respectively, of a Fredholm integral equation

$$\int_D \boldsymbol{\phi}_n(\mathbf{r}_1, \omega) \boldsymbol{\mathcal{W}}(\mathbf{r}_1, \mathbf{r}_2, \omega) \, \mathrm{d}^3 r_1 = \lambda_n(\omega) \boldsymbol{\phi}_n(\mathbf{r}_2, \omega). \tag{2.26}$$

Thus, we can express the (electric) cross spectral density tensor $\boldsymbol{\mathcal{W}}$ as an uncorrelated sum of completely coherent modes

$$\boldsymbol{\mathcal{W}}_n(\mathbf{r}_1, \mathbf{r}_2, \omega) = \lambda_n \boldsymbol{\phi}_n^\dagger(\mathbf{r}_1, \omega) \boldsymbol{\phi}_n(\mathbf{r}_2, \omega). \tag{2.27}$$

Similarly to the scalar case, the (electric) cross-spectral density tensor can be represented as a correlation function of the form

$$\boldsymbol{\mathcal{W}}(\mathbf{r}_1, \mathbf{r}_2, \omega) = \langle \mathbf{F}^\dagger(\mathbf{r}_1, \omega) \mathbf{F}(\mathbf{r}_2, \omega) \rangle, \tag{2.28}$$

where functions $\mathbf{F}$ can be understood as space–frequency domain realizations of the electric field. Modes $\boldsymbol{\phi}_n$ can be used in modeling optical systems by propagating them through optical systems and superposed incoherently after the system. It should be noted that defining the cross-spectral density separately for each polarization component of the electric field using the scalar approach leads to a solution of the diagonal elements only, while the off-diagonal elements would remain unknown. This approach is clearly inadequate for rigorous analysis of coherence properties of electromagnetic fields. Rigorous analysis of partially coherent vectorial fields requires electromagnetic coherent-mode decomposition [46]. Analytic expressions of some specific types of partially coherent beams,

such as Gaussian Schell-model beams, where the intensity and the degree of coherence are both Gaussian, can be found in the literature [47].

2.3 POLARIZATION

Let us consider the simplest solution to the Helmholtz equation, a random or deterministic plane wave, propagating in positive z-direction, and expressible in the form

$$E(\mathbf{r},\omega) = \{E_{0x}\hat{\mathbf{x}}\exp[\mathrm{i}\phi_x(\omega)] + E_{0y}\hat{\mathbf{y}}\exp[\mathrm{i}\phi_y(\omega)]\}\exp(\mathrm{i}kz). \quad (2.29)$$

Here E_{0x} and E_{0y} are amplitudes, $\hat{\mathbf{x}}$ and $\hat{\mathbf{y}}$ are unit vectors, $\phi_x(\omega)$ and $\phi_y(\omega)$ are the phase terms of the electric field components vibrating in the x- and y-directions, respectively, at frequency ω, and $k = 2\pi/\lambda$ is the wave number. Polarization is a term that is used to describe the relations of the phases and amplitudes of the orthogonal electric field components. If only one of the components is nonzero or the phase difference between the two components $\delta = \phi_y - \phi_x$ is a multiple of π the field is linearly polarized. When both of the components are nonzero and the phase difference δ is not a multiple of π, the field is said to be elliptically polarized. A special case of this is $|E_x| = |E_y|$ and $\delta = \pm\pi/2 \pm 2m\pi$, when the field is said to be circularly polarized. As the polarized field propagates, the end point of the electric field vector traces out a characteristic form according to the polarization state. This trace is generally an ellipse, thus in the case of circular polarization it forms a circle and in case of linear polarization a line.

2.3.1 Jones matrix formalism

Let us rewrite Eq. (2.29) in the form

$$\mathbf{E}(\mathbf{r}) = (E_x\hat{\mathbf{x}} + E_y\hat{\mathbf{y}})\exp(ikz) = \begin{bmatrix} E_x \\ E_y \end{bmatrix}\exp(\mathrm{i}kz), \quad (2.30)$$

where E_x and E_y are complex constants. The column vector in Eq. (2.30) is called the Jones vector [48–50] and is classically denoted

by **J**. For simplicity the Jones vectors **J** can be normalized by demanding that $|E_x|^2 + |E_y|^2 = 1$. As the absolute phase is usually not significant factor compared to the phase difference between the two components, it is customary to set the phase of the E_x component equal to zero. For example linear polarization in x-direction can be expressed in the form

$$\mathbf{J} = \begin{bmatrix} 1 \\ 0 \end{bmatrix}. \tag{2.31}$$

Analogously various optical elements can be described by 2 x 2 Jones matrices. The Jones vector behind some optical element $\mathbf{J}_{\text{out}}$, described by Jones matrix say **M**, can be expressed by a simple matrix multiplication

$$\mathbf{J}_{\text{out}} = \mathbf{M}\mathbf{J}_{\text{in}}. \tag{2.32}$$

2.3.2 Partial polarization

Jones calculus, described in the previous section, can only be used to model completely polarized fields. Analysis of partially polarized fields requires us to define polarization using results defined earlier for coherence theory. Let us consider plane-wave-like and stationary (at least in wide sense) electric field $\mathbf{E}(t) = [E_x, E_y]^T$, where t is time and E_x and E_y are x and y components of the electric field analogous to Eq. (2.29). Polarization state of the field may be expressed using Stokes parameters [51, 52], that are defined in the form

$$S_0 = \langle E_x^* E_x \rangle + \langle E_y^* E_y \rangle = \langle I_x \rangle + \langle I_y \rangle, \tag{2.33}$$

$$S_1 = \langle E_x^* E_x \rangle - \langle E_y^* E_y \rangle = \langle I_x \rangle - \langle I_y \rangle, \tag{2.34}$$

$$S_2 = \langle E_x^* E_y \rangle - \langle E_y^* E_x \rangle = 2\langle E_{0x} E_{0y} \cos\delta \rangle, \tag{2.35}$$

$$S_3 = \mathrm{i}(\langle E_y^* E_x \rangle - \langle E_x^* E_y \rangle) = 2\langle E_{0x} E_{0y} \sin\delta \rangle, \tag{2.36}$$

where $\langle\rangle$ denotes time averaging. For convenience, the Stokes parameters may be normalized by S_0. These are later denoted by small symbols. It is clear from Eqs. (2.33) and (2.34) that terms S_1 and

S_2 represent the sum and difference of the intensities of orthogonal polarization components, hence S_1 is a measure of the degree of linear polarization in coordinates described by the orthogonal electric field components. The term S_2 illustrates the degree of linear polarization at coordinates rotated by 45 degrees compared to the original coordinate system and S_3 is a measure of circular polarization.

Obviously, if the field consists of a single monochromatic plane wave component, the degree of polarization is unity. Let us next consider a field consisting of mutually uncorrelated plane-wave-like components defined as in Eq. (2.29) with different angular frequencies, with bandwidth of $\Delta\omega$. Different frequency components of the field may have different phase differences δ leading to partial polarization according to Eqs. (2.33)-(2.36). The Stokes parameters can be measured with relatively simple optical setup [53, 54]. The degree of polarization can be expressed by means of Stokes parameters as

$$P = \frac{\sqrt{S_1^2 + S_2^2 + S_3^2}}{S_0}. \tag{2.37}$$

Alternatively the degree of polarization can be determined by using the mutual coherence matrix defined in Eq. (2.14), and the degree of polarization takes the form [26]

$$P = \sqrt{1 - \frac{4 \det \mathbf{\Gamma}(0)}{[\mathrm{tr}\mathbf{\Gamma}(0)]^2}}, \tag{2.38}$$

where det and tr denote the determinant and the trace operator, respectively. Definition in Eq. (2.38) implies, that the degree of polarization is a measure of correlation between the orthogonal electric field components at a single point [55]. The degree of polarization can be analogously derived from the cross-spectral density matrix in space–frequency domain [52].

Perhaps the most descriptive way of representing the polarization state is the Poincare sphere in Fig. 2.1. The Poincare sphere is a unit sphere with axes defined by normalized Stokes parameters

s_1, s_2, and s_3. Any polarization state can be expressed as a vector starting from origin in Poincare sphere. The length of the vector is defined by the degree of polarization and the direction of the vector defines the polarization state. Any polarization vector ending at the perimeter of the sphere represents complete polarization. The north and south poles denote right- and left-handed circular polarization, respectively, and all states of linear polarizations are located in the equator. Other elliptical polarization states occupy the rest of the surface of the sphere. All partially polarized states lay inside the sphere and the completely unpolarized state is at the origin. Using spherical coordinates illustrated in Fig. 2.1, the normalized Stokes parameters can be written as [55]

$$s_1 = P\cos(2\psi)\cos(2\chi), \tag{2.39}$$

$$s_2 = P\cos(2\psi)\sin(2\chi), \tag{2.40}$$

$$s_3 = P\sin(2\psi). \tag{2.41}$$

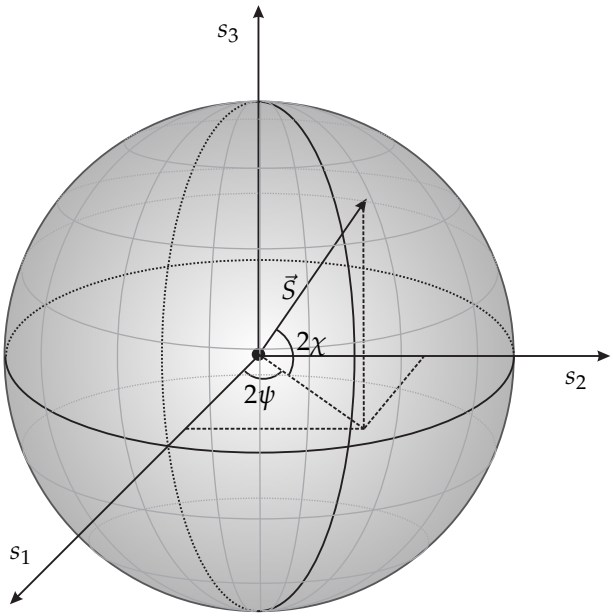

Figure 2.1: Illustration of the Poincare sphere.

3 Diffractive optical elements

Diffraction grating refers to a periodically modulated physical property in material that affects the propagation of waves [20,56,57]. The modulation is seen as a change in the permittivity, and it can be produced by modulating either the surface of the material (surface-relief gratings) or the permittivity inside the material (volume gratings). The first references to diffraction gratings are dated to the 16th century, when D. Rittenhouse fabricated the first known grating from hair positioned by the threads of two screws [58].

Probably the most renowned experiment demonstrating the existence of diffraction is Young's double slit experiment, where two wavefronts originating from two pinholes form a diffraction pattern on a screen far away from the slits. The physical interpretation of the experiment was given by Huygens already in the 17th century. Huygens stated that the slits can be imagined as two point sources. The wavefronts behind the slits are in phase only at discrete angles. At these directions the waves interfere constructively and diffraction maxima can be observed. Destructive interference takes place at the directions in which the wavefronts are out of phase resulting in intensity minima at the observation plane.

This chapter defines the properties of surface-relief diffraction gratings and the method for analyzing grating problems used in this thesis. The main features and applications of two special types of gratings, namely guided-mode resonance and polarization division gratings are discussed in more detail.

3.1 DESIGN

Figure 3.1 illustrates the principle of the diffraction by a two-dimensional surface-relief grating. The directions of the propagating diffraction orders can be easily calculated by using the grating

equation [20]

$$n_1 \sin\theta_1 = n_3 \sin\theta_3 + m\lambda/d, \tag{3.1}$$

where m denotes the diffraction order. The grating equation tells us only the directions of all possible propagating diffraction orders, but gives no information about the amplitude or phase of the orders. To solve the grating problem rigorously, we need to consult Maxwell's equations.

Gratings can be divided into three sub-groups with different characteristics originating from the ratio between the period and wavelength. The domains are paraxial $(d \gg \lambda)$, resonance $(d \approx \lambda)$, and quasi-static $(d \ll \lambda)$ [20]. In the paraxial domain, the response of the grating is almost independent on the polarization and it can be treated as a thin transparency. In the resonance domain the polarization has significant impact on the function of the structure. Finally in the quasi-static domain, the structure acts as an uniform anisotropic layer with effective refractive index. The latter are also called zeroth-order gratings as only the zeroth transmitted and reflected orders are allowed to propagate outside the grating. The

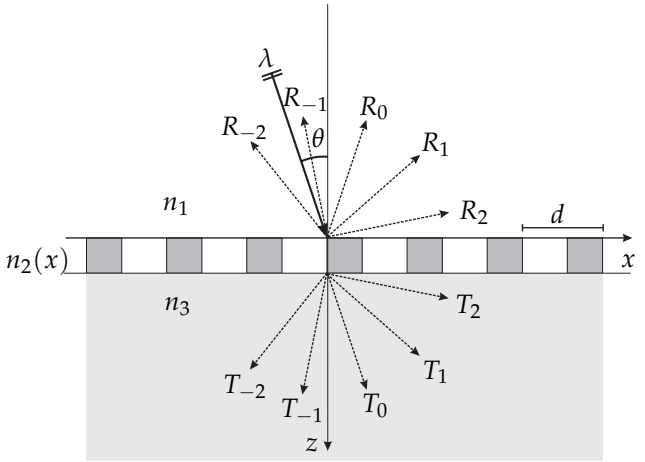

Figure 3.1: Schematic diagram of diffraction. Incident plane wave arrives to the modulated layer in an angle θ, and is split to transmitted (T_m) and reflected (R_m) diffraction orders. d illustrates the period of the structure, λ is the wavelength of the incident wave and n_i denotes the refractive index in different layers.

structures considered in this work fall in the resonance domain, i.e., the wavelength and period of gratings are at the same order of magnitude. We are thereby forced to apply a rigorous treatment of the problem.

Let us consider a plane wave incident at the grating layer. If the field is of a more general form, we may divide it into the angular spectrum [26] that consists of plane wave components with different complex amplitude vectors and wave-vectors. The grating structure is generally divided into layers having invariant permittivity in z-direction (complex refractive index) similarly to Fig. 3.1. The grating in Fig. 3.1 consists of only one modulated layer denoted by subscript 2. Maxwell's equations are formed at each layer, resulting to a system of equations for both orthogonal polarizations. By combining these equations within the group leads to so called basic equations for both polarizations. The basic equation that contains only the y-component of the electric field, also called transverse electric or TE polarization, closely resembles the Helmholtz equation, whereas the equation that includes only the y-components of the magnetic field, known as transverse magnetic or TM polarization, differs from it.

As we consider periodically modulated permittivity in grating layer, it follows from famous Bloch (or Floquet–Bloch) theorem [59], that the output field is pseudo-periodic. Therefore we may express the permittivity and the field as Fourier and pseudo-Fourier series, respectively. These equations are then transferred to a matrix-eigenvalue problem that is used to solve the propagation constants of the diffracted angular spectrum components. The field is then expressed as a sum of forward and backward propagating modes with yet unknown complex weights. Boundary conditions are then used to connect the fields at boundaries of discontinuity. This can be expressed as a block-matrix equation connecting the fields at adjacent layers.

Generally there are no analytical solutions for the problem, except for some special cases such as a plane wave at planar boundary that leads to Fresnel's coefficients [55]. Hence we are forced

to solve the problem numerically. There are several methods to perform this. Here we use Fourier Modal Method (FMM) [60, 61] applying recursive scattering matrix (S-matrix) [62–64] to solve the boundary value problem. The use of FMM with S-matrix approach has become a standard tool in solving grating problems, and after strong contributions in developing the method by Li [61, 64] and others [65–67] it can be used quite safely in most cases. The procedure presented above is described in great detail in [61, 63, 64, 68].

3.2 RESONANT WAVEGUIDE GRATINGS

There are two grating anomalies referred to Wood's anomalies, namely Rayleigh and resonance type [69–73]. The term resonant grating refers to sharp peaks in the reflection spectra of the structure due to strict coupling condition. Rayleigh's anomaly takes place in the grazing angle, i.e., at least one propagating diffraction order is parallel to the grating vector. Resonance anomalies occur when electric field is coupled to a waveguide that supports the grating coupler. The resonance waveguide grating (RWG) can also consist of solely the grating layer with high effective refractive index that acts as a coupler and supports the guided mode. These structures, also called guided mode resonance gratings GMRG [74], have drawn much attention lately. RWGs have been applied as wide band [75, 76] and narrow band [77] filters, polarizers [78] and laser mirrors [79, 80]. In guided mode resonance, all the incident energy is transferred to 0^{th} reflecting diffraction order at a frequency band that can be tailored by the design of the structure.

Recently enhancing the light matter interaction e.g., in Raman spectroscopy [81,82] and fluorescent measurements [83] has become an interesting field for RWGs. The sensitivity is increased, since in the RWG the incident wave is coupled into a waveguide mode that propagates in this modulated waveguide for microns [84] before escaping from the waveguide. Compared to the structural thickness, the interaction length is greatly increased leading to a strong increase in the sensitivity of the measurements. Moreover, the local

field is enhanced in the grating layer leading to an even greater increase of field matter interaction. Figure 3.2 illustrates the principle of RWG.

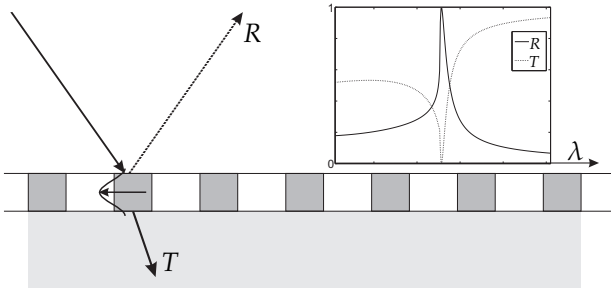

Figure 3.2: Illustration of resonant waveguide grating. Incident wave is guided to leaky waveguide mode and reflected to 0^{th} reflected diffraction order. Inset represent typical response of RWG.

The effective refractive index of the waveguide layer has to be higher than in the surrounding layers for guided mode resonance to take place. Modeling of the resonance domain structures has been studied quite intensively during the past few decades [85–87]. Requirements for guided mode resonance can also be calculated by modeling the waveguide as an uniaxial crystal. This yields to regimes generally different for perpendicular polarization component in which the resonance may occur [76]. Even though this analysis gives an ideal starting point for analyzing RWGs, in this thesis we focus on using FMM for solving the problem rigorously. This is justified also since we are interested in the phases or phase differences of different field components.

3.3 POLARIZING SUB-WAVELENGTH STRUCTURES

Polarizing structures refer to elements that separate different polarization components, ideally leading to completely polarized signals. This can be obtained by using well-known wire-grid polarizers [88, 89], resonant waveguide gratings introduced in previous section, space-variant polarization gratings [54], or recently intro-

duced inverse polarizers [90]. Figure 3.3 illustrates probably the most typical sub-wavelength polarizing structure, a wire-grid polarizer. Physically the operation of such a device can be explained by interaction between free electrons in metallic wires and the electromagnetic field. The field makes the free electrons inside the wires to oscillate along the field. The movement of the electrons is quite free along the field component parallel to the wires and the field experiences the grating layer similarly to a bulk metal layer and is thus reflected. However, the electrons are bound in direction perpendicular to wires and the field perpendicular to wires experiences the layer as a dielectric film.

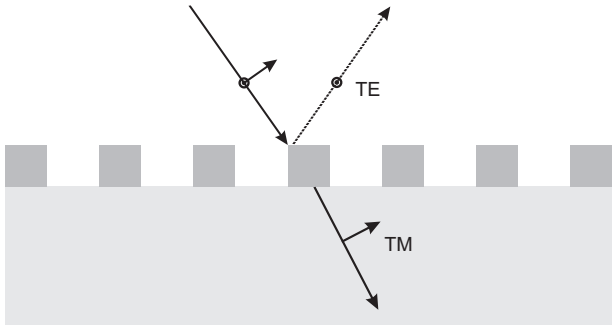

Figure 3.3: Cross-section of a wire-grid polarizer showing the effect for perpendicular field components, and the name convention of the electric field components, in which TE is perpendicular and TM is parallel to the plane of incidence.

Polarization gratings are specific types of sub-wavelength structures that spatially modulate the polarization state of the incident electric field. There are two main categories of polarization gratings, namely structures that modulate spatially the amplitudes of incident polarization states and structures that spatially modulate the phases of the polarization components. The first type of structures can be produced by wire-grid polarizers with spatially varying fringe direction [54], whereas the latter consist of spatially varying wave plates [91]. Experimental results of fabricated polarization gratings based on both concepts are presented in detail in [**II**]. Let us consider a structure that consists of sub-wavelength fringes rotat-

ing by linear law in the x-direction. If we use the notation described by [91] the efficiencies of three central diffraction order take on the forms

$$\eta_0 = \frac{1}{4}|A+B|^2, \tag{3.2}$$

$$\eta_{\pm 1} = \frac{1}{8}|A-B|^2\left[1 \pm \frac{2|E_x||E_y|\sin(\Delta\theta)}{|E_x|^2+|E_y|^2}\right], \tag{3.3}$$

where A and B denote the complex-amplitude transmission coefficients of the local fringes for TE and TM components of the electric field, respectively. Moreover, E_x and E_y denote the cartesian components of the incident field, and $\Delta\theta = \arg E_x - \arg E_y$ is the phase difference. Gori [54] showed that the polarization state of the zeroth diffraction order is identical to that of the incident wave, whereas diffraction orders -1 and 1 are right and left handed circularly polarized, respectively. As can be seen from Eq. (3.3), beam splitters with desired value of energy to three central diffraction orders can be designed by tailoring the grating parameters and the incident electric field.

The term inverse polarizer refers to a structure where the transmission efficiency of the TE-component exceeds the TM-component that is either reflected and/or absorbed by the structure. Inverse polarization can take place in thin metallic gratings, where the period of the structure is the same order of magnitude as the illumination wavelength. This makes the fabrication of these elements more straightforward compared to the classical polarizers, that generally consist of metallic wires in the quasi-static domain. The transmission of the TE polarization is due to the low absorption of the thin metallic structure [90] or by guidance the polarization to a low-loss metal-insulator-metal waveguide. The suppression of the TM polarization is based on grating resonances such as Wood's anomaly [90] or excitation of localized surface plasmon polaritons [**III, IV**]. The presence of grating anomalies, that are obligatory for the operation of these structures, makes them extremely sensitive to fabrication and mounting errors and they generally are effective only for a narrow wavelength band.

4 Fabrication

Diffractive optical elements have gained more and more ground in commercial applications during the past few decades. The invention and development of laser initiated the commercialization of these structures in consumer electronics. Nowadays interference lithography can be used for fabrication of structures with periods less than 100 nm [92]. Fabrication of diffractive optics has adopted methods from electronics industry [93], e.g. electron beam lithography (EBL) [18, 94], that still is far too cost-inefficient method for commercial direct write applications. However, EBL provides a flexible concept for fabricating complex structures with best achievable resolution in relatively large size, ideal for research purposes. Moreover, structures fabricated using EBL can be mass produced in good extent using techniques such as nanoimprint lithography [95] and UV and hot embossing.

In this chapter, the fabrication methods used in this thesis are described in detail. Aluminum processing is given special attention, since a careful optimization of the process enabled experimental results presented in papers **II–IV.**

4.1 ELECTRON BEAM LITHOGRAPHY

Pattern generation in EBL is based on scanning an electron beam on material sensitive to the electron irradiation. The chemical composition of the material, also called resist, is altered due to the absorbed energy from the beam. This enables dissolution of either the exposed or the unexposed area by a proper chemical, called the developer. Pattern generated into the resist can now be used in post-exposure processes described in more detail in the next sections. Electron beam is generated using a thermal field emission gun, or by thermionic emission and the beam is aligned and focused on sample surface using magnetic coils and two or more

magnetic lenses. In this work we used a vector scanning system, in which the beam is deflected with magnetic deflection coils to pattern an area called the main field without moving the stage. If structure with size larger than the main field is required, stage is moved to the center of the next main field with high precision using interferometric stage measurement system and the new main field is exposed. This procedure is called stitching. The exposure dose is determined by the beam-on time before blanking and deflection of the beam. Figure 4.1 illustrates a typical column assembly.

The first commercially available scanning electron microscopes were launched in 1965 by Cambridge Scientific Instrument Company. Soon after this these devices were converted for electron beam lithography purposes by adding a beam blanking unit, a pattern generator, and interferometric stage controlling unit. Nowadays there are several systems designed and dedicated solely for pattern generation purposes, with high speed blanking units and precisely controlled stages that makes it possible to stich main fields accurately together forming large area exposures. All the structures described in this work are exposed using Vistec EBPG5000+ES HR,

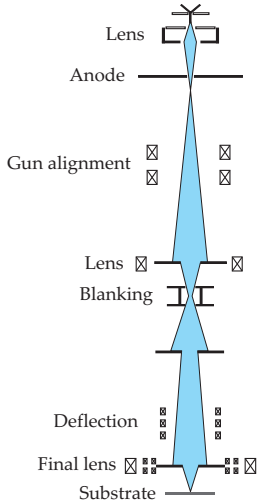

Figure 4.1: Schematic of a Vistec EBPG column showing the main elements for alignment and focusing of the beam.

that is vector scanning Gaussian beam system operating at 20, 50, or 100 kV acceleration voltage, with 50 MHz pattern generator. Gaussian beam system is the most common choice for the research and development, since the resolution is better compared to variable shaped beam systems, that outperform the Gaussian beam systems in terms of throughput.

4.2 RESIST TECHNOLOGY

Electron beam resists are divided into two categories based on the resist behavior during the development. If the exposed areas are diluted during the development, the resist is called a positive tone resist. Analogously, if the unexposed areas are diluted during the development, the resist is called a negative tone resist. There are many different kinds of positive and negative tone resists, each with their own characteristics by means of required dose, achievable resolution, and etch resistivity in selective etching processes that are described later. The resists used in the structures described in this thesis are polymethyl methacrylate (PMMA) [96] and ZEP 7000-series resist from Zeon Corporation, that is a styrene/chloromethyl acrylate copolymer dissolved in digmyne (bis(2-methoxyethyl)ether). Both are positive tone resists with relatively high resolution.

The resist layer is applied on the substrate by spin, spray, roll, or dip coating. The used method depends usually on the application, but probably the most practical method for coating flat substrates uniformly is spin coating. After the resist is spun to the substrate, it is usually soft baked to remove the solvent from the layer. Additional thin metallic layer (few tens on nanometers) may be applied on the resist to prevent the sample from charging during the exposure.

4.3 LIFT-OFF

Lift-off [97] is probably the most straightforward method for fabricating structures in nano- and micrometer scale. The structure is

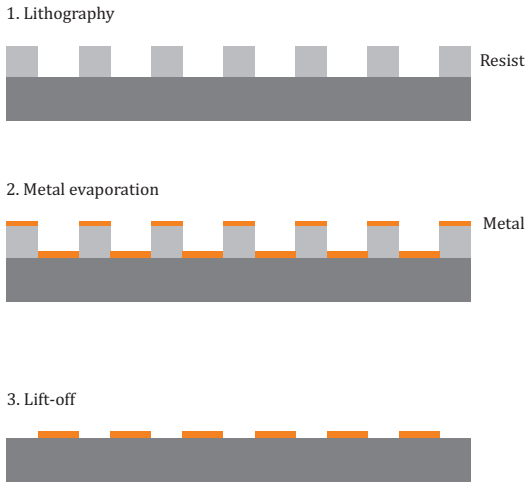

Figure 4.2: Lift-off process.

defined in lift-off by depositing material (usually metal) on resist structure fabricated by some lithography method. The deposition has to be highly directional to minimize the deposition on the sidewall. This makes physical vapor deposition (PVD) extremely suitable for the process. Resist structure is stripped away using suitable solvent, and the deposited material is preserved only on the areas that were open on the substrate. Figure 4.2 illustrates the principle of lift-off. Even though lift-off is a robust method for producing features with extremely fine features, it has limitations such as limited structure height and aspect ratio determined by the ratio between the height and line width of the structure.

PMMA was used as a lift-off resist for the structures defined in paper **II**, and it was dissolved with acetone (AC). Dissolution was improved by heating the solvent and the sample to 40°C and by small agitation in ultrasonic path.

4.4 REACTIVE ION ETCHING

After the structure is successfully generated into the resist, it needs to be transferred to the substrate. This can be done by etching,

in which the material is removed selectively in the areas defined by the etching mask. There are both wet and dry etching methods for different purposes. Generally the wet etching processes are isotropic, referring to a constant etching speed in all directions (some crystalline material such as silicon can be etched selectively, with direction defined by the crystalline orientation), whereas the dry etching can be highly directional or anisotropic. Reactive ion etching (RIE) [98] is a dry etching method, in which plasma containing charged particles initiated by a strong radio frequency (RF) field are accelerated and collided to the surface of the sample. RIE process can be separated to two main types that may take place simultaneously: physical and chemical etching. In physical etching, also called sputtering, the ions remove material by a simple collision force. Therefore it is highly directional and quite anisotropic. Physical etching results to a low selectivity between the mask and the target material because the collisions to the surface remove also the mask material.

The chemical etching is based on the chemical reactions between the etchant and the target material. The chemical etching is normally very selective because the etchant can be selected so that it reacts only with the target material. Chemical etching is also quite isotropic because the chemical reactions also occur in the horizontal direction. In order to produce highly selective etching process one has to control both the physical and the chemical parts of process. Optimization of dry etching processes is described in the next two subsections for two different materials.

4.4.1 Silicon nitride etching

Nitrides as well as oxides can be etched using fluorine containing gases. Typically the chemical part in these processes is CHF_3, CF_4, or SF_6, and the physical etching is performed by adding O_2, He, or Ar to the gas mixture. Si_3N_4 structures described in paper **II** were etched using CHF_3/O_2 chemistry similar to that in [99]. O_2 addition suppresses the formation of fluorocarbon on nitrile layer that slows

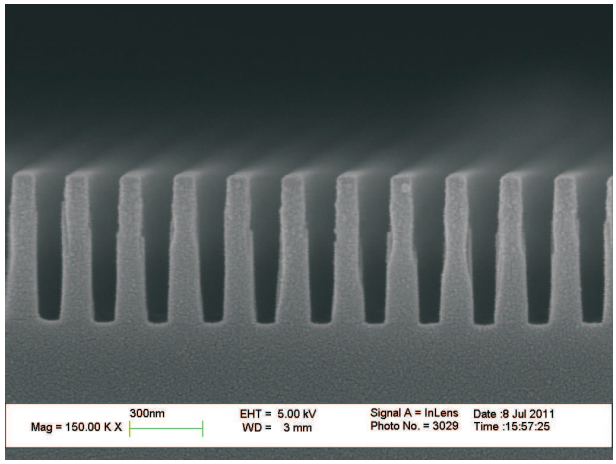

Figure 4.3: Cross-section of the Si_3N_4 grating etched with the optimized process.

down the Si_3N_4 etch rate [100]. Oxygen addition also increases the etch rate of the resist resulting to the decrease in the selectivity using the resist mask in Si_3N_4 etching. Therefore a metallic etching mask is required. Figure 4.3 shows the profile of the Si_3N_4 grating etched with the optimized process.

4.4.2 Aluminum processing

Aluminum (Al) thin films are deposited by PVD [101] using electron gun in a high vacuum chamber. PVD is a general term for the thin film deposition process in which the target material is vaporized and the vapor is condensated to the substrate. There are several different methods to vaporize the target material which include electron beam, high current, pulsed laser, and plasma discharge. Throughout this thesis, we use only electron beam and electric current PVD. In electron beam PVD, the pure target material is heated by bombarding the target with electrons. The beam is also usually wobbled to guarantee uniformity. The deposition speed can be controlled by current of the beam. In the electric current PVD, the target material is placed to a container with high electric resistance. As the electric current is increased, the target material starts

to evaporize. The parameters that mostly effect on the quality and properties of the evaporated layer are: purity of the target material, the vacuum level, evaporation speed, and the temperature of the substrate.

Al easily forms aluminum oxide and therefore high vacuum is required to form good aluminum thin film. The quality of the film can be improved by increasing the vacuum level during the deposition or by increasing the deposition speed. Titanium and chromium can be used for gettering by absorption to improve the vacuum level even further [102,103]. Both of the materials were used successfully to improve the vacuum level prior to the Al deposition. As the deposited aluminum film is exposed to air it naturally forms a thin aluminum oxide layer on the aluminum. This can be avoided by deposition of a thin film on the Al layer during the deposition cycle which blocks the oxidation. In this thesis we used silicon dioxide (SiO_2) that also serves as an etching mask for the aluminum. In addition to good selectivity, SiO_2 mask improves the etched Al profile by sidewall passivation [104].

For Al etching, we developed a highly anisotropic etching process for fine Al features based on three different gases, all of which incorporate different mechanism in the process. The main etchant for Al is chlorine (Cl_2). The aluminum oxide was removed with BCl_3 that is also the physical etching gas in the process. Small amount of O_2 was added to the gas mixture for preserving the SiO_2 mask and for preventing horizontal etching of Al. The ratio between the Cl_2 and BCl_3 is used to control the amount of chemical and physical etching. The O_2 ratio is tuned so that the line widths are preserved during the etching by depositing a thin passivating aluminum oxide layer to the sidewalls of the structure [105]. The passivating layer withstands the bombardment with BCl_3 due to the direction of the reactive ions. The O_2 flow has to be small enough so that the oxide forming on the vertical surfaces is removed by the BCl_3 bombardment. The line widths of the structures can be slightly modified by the O_2 flow.

Figure 4.4 illustrates the effect of O_2 addition to the Al etching

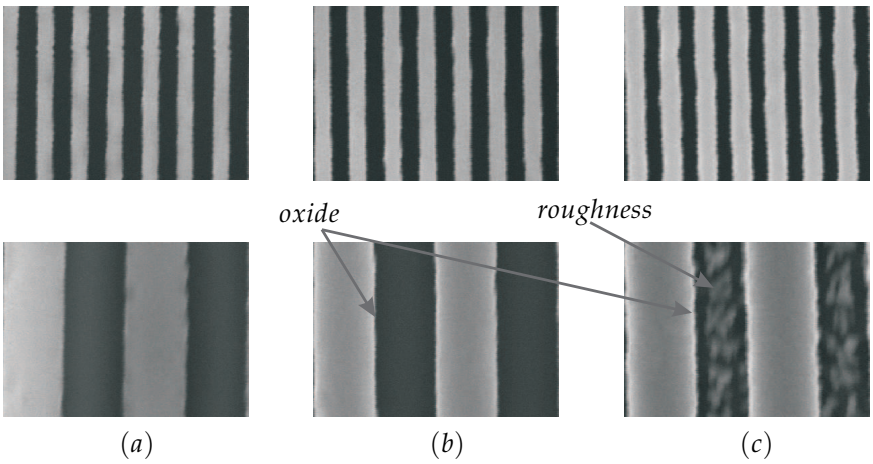

Figure 4.4: SEM-images of aluminum structures etched with different O_2 flow: (a) 0 sccm, (b) 1 sccm, and (c) 2 sccm. The periods in the upper images are 150 nm and 500 nm in the lower images.

process. The increase of O_2 flow leads to more charging in the SEM-image due to the formation of aluminum oxide which can be easily seen by the increase of brightness from Fig. 4.4 as a function of O_2 addition. The increase of the O_2 flow leads to an increase of the line width and finally appearance of roughness on the grating grooves often referred as "grass". If the oxygen flow is increased further, the formed oxide layer is no longer removed by BCl_3 and the etching is stagnated. Figure 4.5 illustrates the SEM-image of the cross-section of aluminum wire-grid etched using the optimized process.

As a conclusion, we can state that the etching of structures with extremely small feature sizes requires passivation of the side wall to maintain the critical dimension. In the case of Al etching, this can be done by adding small amount of O_2 to the etching gas mixture. The optimized recipe contains 1 sccm (standard cubic centimeter) of O_2 in addition to Cl_2 and BCl_3. Naturally the optimal etching recipe depends on the characteristics of the deposited aluminum and the used equipment for etching. For example, we noticed that for sputtered aluminum, the optimal recipe is completely different due to the different composition of the Al layer. However, the re-

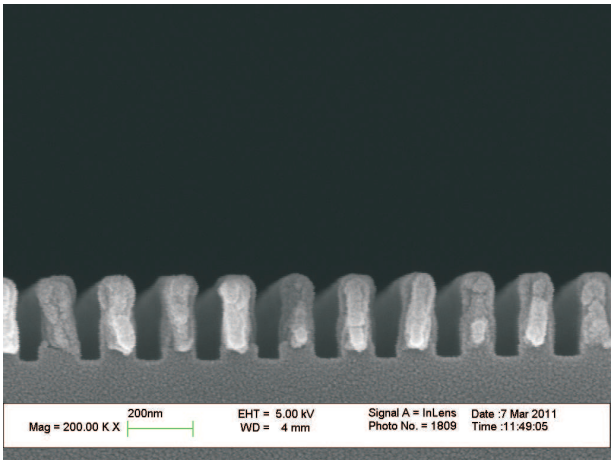

Figure 4.5: SEM-images of a cross-section of an aluminum grating etched with optimized process described above.

sults described above may be used as guidelines for optimization of Al etching recipe. In our experiments we used Plasmalab 100 (Oxford Instruments) for aluminum etching.

4.5 SUMMARY

The main fabrication methods used in this thesis were described. Electron beam lithography was shown to provide optimal tool for research purposes in lithography in terms resolution, flexibility of patterns, and robustness.

Two methods for transferring the resist pattern to metallic structure, namely lift-off and dry etching were described. Whereas the lift-off offers a robust transfer technique regardless of material, it lacks the capability to be used for fabricating structures with high-aspect ratio. Even though optimization of dry etching processes requires much more effort, as it is optimized, it provides achievable aspect ratios superior to lift-off. The represented Al etching recipe can be used for fabricating extremely fine features into Al. In addition, it is suitable for etching features with various dimensions by tuning the O_2 flow: for larger features less O_2 is added

to gas mixture to maintain high etching speed and clean grooves, whereas with finer features, more O_2 is needed to preserve critical dimensions. Etching of Si_3N_4 structures with aspect ratio exceeding 5 were presented. These aspect ratios are required to introduce the phase delays of orthogonal polarization components discussed in the Chapter 5.

5 Main results

The main results of papers **I–V** are explained briefly in this chapter. Depolarization of quasi-monochromatic and spatially partially coherent light by resonant gratings, i.e., the results of papers **I** and **V**, respectively, are discussed in section 5.1. Papers **II–IV** that deal with polarization division, each from different aspects are discussed in section 5.2.

5.1 DEPOLARIZATION BASED ON RESONANCE GRATINGS

Sub-wavelength linear gratings, especially in resonance domain, have significant difference in the effective refractive index of the two perpendicular polarization components in the grating layer. Therefore the grating resonances generally take place with different grating configurations for different polarization states. Let us again assume the incident field to consist of plane wave components with bandwidth $\Delta\omega$. Furthermore, let us assume, for simplicity, that the spectral density $S(r,\omega)$ is constant over this interval. Thus we assume that all plane wave components have equal amplitudes. By examining Eqs. (2.14) and (2.38) it becomes clear that for achieving complete depolarization, the perpendicular polarization components need to have equal amplitudes and the correlations of the TE and TM polarizations need to be suppressed. This means that the off-diagonal elements of the mutual coherence matrix need to cancel each other out. Solving the system of equations formed by setting the normalized Stokes parameters s_1, s_2, and s_3 to zero, and solving the field components from Eqs. (2.33)$-$(2.36), leads to an analogous conclusion. One possible solution is that the phase difference of the field components vary the amount of $n2\pi$ pitched at uniform intervals.

By optimizing the grating parameters carefully in the total-internal-reflection configuration, one of the polarization components is

guided into a leaky mode and the other is reflected due to the configuration. This leads to a significant temporal delay between the components and, ideally, to complete depolarization. In paper **I** this is studied more carefully for temporally partially coherent incident illumination with numerical examples that show the possibility to depolarize quasi-monochromatic light by using RWGs. We presented results for quasi-monochromatic light, namely for bandwidths of 0.1 and 10 nm. The tolerances become strict for the smaller line widths due to the longer coherence length. This would require longer propagation distance in the corrugated waveguide, which is hard to achieve. Increasing the line width further from 10 nm finally leads to a situation in which every wavelength is not coupled into the waveguide.

In paper **V** we showed that depolarization of spatially partially coherent light can occur in RWG with similar configuration as that presented in paper **I**. As a numerical example, we used the Gaussian Schell-model beam, that has Gaussian characteristics with respect to intensity and spatial coherence. For simplicity we restricted to a one-dimensional GSM field in the analysis. Almost complete transformation from spatially partially coherent, fully polarized input to completely depolarized output was achieved. Physically depolarization of a spatially partially polarized field is almost analogous to the quasi-monochromatic case. The requirement of equal amplitudes of perpendicular polarization components is satisfied by illuminating the RWG using total-internal-reflection configuration, and the different polarization components experience different phase delays in the grating layer. TE- and TM-modes are spatially separated in the transverse plane due to the different propagation distances in the waveguide layer. As we assumed also partial spatial correlation, this leads to a change in the cross-spectral density, and consequently, in the degree of polarization.

5.2 POLARIZATION DIVISION

Paper **II** describes the design, fabrication, and characterization results of surface-relief polarization gratings. Polarization gratings are space-variant structures that spatially modulate the polarization state of light. In Paper **II** we present the results for dielectric blazing structure, triplicator, and metallic polarimeter. If we choose left-circularly-polarized incidence (LCP), and $A = 1$, $B = -1$, and $\Delta\theta = \pm\pi/2$ in Eq. (3.3) we have blazing effect in -1 order that is right-circularly-polarized (RCP). By changing the incident polarization to RCP leads to blazing in order $+1$ analogously reversing the polarization handedness. Let us next assume a linearly polarized incidence. Using the aforementioned carrier-grating parameters, we have a duplicator with $\eta_{-1} = \eta_1 = 1/2$. Moreover, if we choose $A = 1$, $B = \exp(i\theta)$, where $\cos\theta = -1/3$, we have a triplicator with $\eta_{-1} = \eta_0 = \eta_1 = 1/3$. Details of the experiments are described in paper **II**. Figure 5.1 represents a cross-section of the fabricated triplicator.

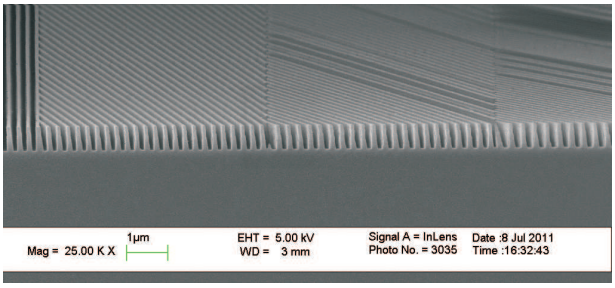

Figure 5.1: SEM-image of the cross-section of the fabricated triplicator from tilted angle illustrating four segments with different fringe orientation.

In paper **II** we also presented results for a polarimeter that is a wire-grid polarizer with linearly rotating transmission axis [54]. We used this polarimeter to measure the Stokes parameters of the diffraction orders of the triplicator also described in paper **II**. The measurement was carried out using the simple method described by Gori [54], that includes measurement of the intensities of the cen-

tral diffraction orders with linear polarizer aligned in two different transmission directions. Since the polarimeter is not ideal due to the fabrication errors, we calculated the scaling factor between the zeroth and $\pm 1^{st}$ diffraction orders that was used to scale the measured intensities. The scaling factor was determined by measuring the intensities of the central diffraction orders from a known linearly polarized incident. Table 5.1 illustrates the measured Stokes parameters of the three central diffraction orders behind the triplicator.

Table 5.1: Measured Stokes parameters and the degree of polarization DOP of the triplicator.

diff. order	s_0	s_1	s_2	s_3	DOP
-1^{st}	1	0.069	-0.011	-0.998	1
0^{th}	1	0.997	0.011	0.035	0.998
1^{st}	1	0.033	0.017	1	1

These results show not only the predicted polarization characteristics of the fabricated triplicator but, more importantly, the functionality of the polarimeter as a robust method for measuring the Stokes parameters.

In Paper **III** we present numerical and experimental results for absorbing polarization-selective gratings, that are based on the enhancement of absorption induced from localized surface plasmons (LSP). Localized surface plasmons are non-propagating coherent oscillations of electrons confined to metallic nanostructures [106, 107]. This resonance leads to strong scattering and absorbance of the electric field at the resonant wavelength. The LSP resonance excited in metals such as gold, silver, platinum, or aluminum is highly sensitive to size, distribution, and shape of the particles. This effect was enhanced by matching the guided mode resonance with LSP to increase the absorption due to extended interaction of the resonant wave with metallic nanoparticles. Introducing guided-mode resonance with LSP leads to even more polarization-selective behavior of the structure.

The structural design of the fabricated element is based on aluminum wire-grid embedded into TiO_2 grown by atomic layer deposition (ALD). This gives us control of the critical parameters required for optimal performance of the device. TiO_2 acts as a waveguide layer, whereas aluminum wires absorb the mode supported by the waveguide. The structure was fabricated using e-beam lithography, and aluminum was processed using the method described in section 4.3.2. Figure 5.2 presents a SEM-image of the cross-section of the fabricated device. The measured results were in good agree-

Figure 5.2: Cross-section of the fabricated absorbing polarization selective grating.

ment with the theory.

Paper **IV** gives some insight in the theory of the inverse polarization effect with experimental demonstration. The fabrication of a standard wire-grid polarizer for UV-wavelengths is extremely challenging due to the small structural dimensions required to approach the quasi-static limit. In addition, the refractive indices of metals become less than ideal for the wire-grid polarizers in the UV. Comparison of materials for wire-grid polarizers shows that the performance of Iridium wire-grid polarizer actually exceeds that of Al wire-grid below wavelength of 300 nm [108]. However, the extinction ratio and the transmission of the TM polarization drops

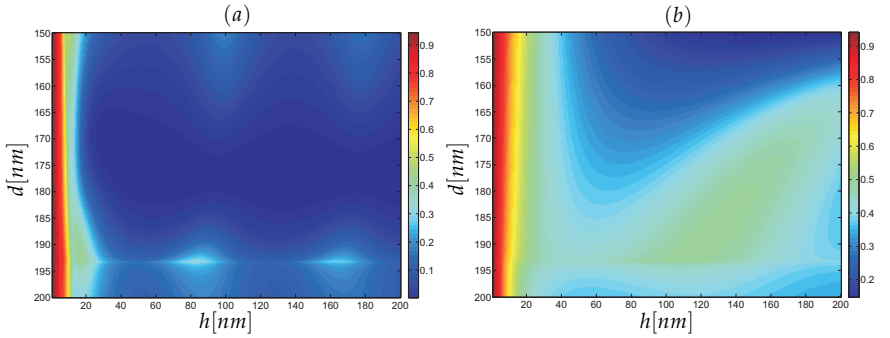

Figure 5.3: Zeroth order diffraction efficiencies of TM (a) and TE components (b) for the optimized inverse polarizer as a function of structure height h and period d.

rapidly and the performance of the Iridium wire-grid becomes poor below 250 nm [108].

We designed an inverse polarizer for 193 nm wavelength. We used FMM to find optimal structural parameters to the extinction ratio of the transmitted field defined as $T_{\mathrm{TM}}/T_{\mathrm{TE}}$ for traditional polarizers and $T_{\mathrm{TE}}/T_{\mathrm{TM}}$ for the inverse polarizers, and transmission efficiency of the transmitted field. Structural design is based on an aluminum ($n_{193\mathrm{nm}} = 0.113 + 2.2062\mathrm{i}$) grid on SiO_2-substrate ($n_{193\mathrm{nm}} = 1.56$). Figure 5.3 illustrates the transmission efficiencies of the TM and TE components of the electric field at a wavelength of 193 nm as a function of structure height and period with fill factor of 0.5 at normal incidence. The optimal period from Figure 5.3 was chosen to be 176 nm. Optimal structural height of about 160 nm would ideally give the best performance. However, in the modeling step we used bulk aluminum refractive index, that is expected to be a bit higher than the refractive index of the evaporated film, and hence we decided to increase the ridge height to 180 nm. This is justified also because of thin native oxide that is grown on the aluminum ridges during etching. By further inspection of the physical operation of the structure, we discovered the structure to act as a metal-insulator-metal (MIM) waveguide. Modal analysis showed that TE_0 and TM_0 modes are both low-loss. This explains the propagation of the TE_0 mode, but does not explain the suppres-

sion of the TM_0 mode. Further analysis showed that the TM mode excites the surface plasmon polariton (SPP) and is guided on the air-metal surface. However, the TE mode does not excite a SPP and it is therefore propagated through the MIM waveguide.

The fabrication of the device was performed using the process described in Chapter 4 and the measurement results were in good agreement with the simulations.

5.3 FINAL REMARKS

We demonstrated theoretically the coherence–polarization mixing using RWGs. Experimental demonstrations of partially correlated fields and especially their interactions with resonance domain structures have not been studied in detail. These interactions may lead to physically interesting discoveries as was shown theoretically in the papers **I** and **V**. The increased use of partially spatially and temporally correlated sources, e.g., in consumer electronics should push this field forward in the near future.

Improving fabrication methods leads to improved material selection and increase of the refractive indices of the materials. Atomic layer deposition (ALD) [109, 110] seems to be a promising method to deposit dense thin films with refractive indices close to those of bulk materials. This improves the tolerances for the plane wave components supported by the waveguide and also gives more freedom in the design of RWGs.

The demonstrated device for measuring the Stokes parameters **[II]** should prove itself useful in characterization of polarization state of relatively coherent sources in the visible wavelength range. The use of partially coherent sources is problematic due to the diffractive nature of the device.

In paper **III** we showed theoretically and experimentally how the guided mode resonance and the localized surface plasmon resonance can be combined. We proposed to use the device for polarization-selective filtering. It should be noted that the structures presented there has a good potential for optical sensing due to the

highly enhanced local electromagnetic field by both the guided-mode resonance and the excitation of LSPs and increased interaction length leading to enhanced light matter interaction.

Physically interesting results of using Al grid as an inverse polarizer for UV was described in paper **IV**. However, experimental use of such a device is limited to low-intensity applications due to the absorption induced heating of the metallic wires. The most interesting application at this wavelength is the optical lithography that is currently used in the processor industry with immersion technique [111]. Therefore it requires a polarizer that is non-absorbing. By designing a linear, sub-wavelength, non-absorbing grating at grazing angle TE- and TM-polarizations can be separated. SiO_2 can be used for the application as it is transparent at this wavelength.

6 Conclusions

Shaping the polarization of light from new perspectives has been studied. Sub-wavelength gratings have been applied to split the signal into different polarization states. Guided-mode resonance gratings are shown to depolarize partially correlated fields due to strong phase shifts induced by the propagation of the modes in the leaky waveguide. Combining guided mode resonance with localized surface plasmons was shown to enhance the absorption owing to increased propagation in the absorbing layer. Inverse polarization effect in sub-wavelength metallic gratings was carefully inspected, giving new physical reasoning for the effect. Numerical and experimental demonstrations were shown to support the theoretical predictions.

The transformation between partial coherence and partial polarization is a physically intriguing phenomenon. This effect, also called coherence–polarization mixing, was shown to take place in RWGs [**I**, **V**]. With proper numerical design, we showed that both spatially and temporally partially coherent sources can be completely depolarized using guided-mode resonant gratings. It would be interesting to study if the depolarization is possible for different distributions of the power spectrum, such as Gaussian distribution. Experimental demonstration of the effect would also be interesting in the future.

Polarization gratings provide means to design lossless beam splitters. The development of lithography processes enables the fabrication of such devices also for visible wavelengths. Polarization gratings are ideally suited for beam splitting applications that require the highest possible diffraction efficiency owing the polarization freedom. These structures were experimentally demonstrated [**II**] with diffraction efficiencies clearly exceeding the limits of the scalar diffraction theory. Moreover, it was experimentally shown that, as predicted, polarization gratings based on the spatial

modulation of the amplitudes of different polarization states can successfully be used as a polarimeter.

In paper **III**, we enhanced the absorption induced by the excitation of localized surface plasmons by guided mode resonance. The structures consisted of gold or aluminum wires embedded in TiO_2 waveguide grating. Almost 100% absorption of one of the polarization components was experimentally achieved with a very thin metallic structure while the perpendicular polarization component was transmitted with low losses. We designed the structure that works as a polarizing beam splitter. The combination of these two phenomena could give rise to greatly enhanced sensing applications at present solely based on LSPs [106, 112]. This certainly is a promising topic for further studies.

Inverse polarizers can be based on different grating anomalies. We designed and fabricated one for deep UV ($\lambda = 193$ nm) based on selective excitation of surface plasmon resonance [**IV**]. This kind of structure suits ideally for low-intensity applications due to heat effects in metallic wires. For high-power applications, polarizers should exploit the birefringence of sub-wavelength gratings.

Albeit the substantial theory provided in this thesis to describe physically the light and matter interactions, the experimental work presented should be regarded equally important. Experimental verification of the theoretical work gives not only credibility to the research but also improves the application sight.

References

[1] I. Vartiainen, P. Vahimaa, and M. Kuittinen, "Analysis of interferograms from a diffractive-lens-based common-path interferometer," *Appl. Opt.* **47,** 5167–5174 (2008).

[2] V. Kalima, I. Vartiainen, T. Saastamoinen, M. Suvanto, M. Kuittinen, and T. T. Pakkanen, "UV-curable ZnS/polymer nanocomposite for replication of micron and submicron features," *Optical Materials* **31,** 1540–1546 (2009).

[3] M. Karlsson, I. Vartiainen, M. Kuittinen, and F. Nikolajeff, "Fabrication of sub-micron high aspect ratio diamond structures with nanoimprint lithography," *Microelectronic Engineering* **87,** 2077–2080 (2010).

[4] G. Kang, I. Vartiainen, B. Bai, and J. Turunen, "Enhanced dual-band infrared absorption in a Fabry-Perot cavity with subwavelength metallic grating," *Opt. Express* **19,** 770–778 (2011).

[5] G. Kang, I. Vartiainen, B. Bai, P. Pääkkönen, and J. Turunen, "Compact middle-wave infrared Fabry–Perot interferometer with double metallic subwavelength gratings," *Opt. Lett.* **36,** 1011–1013 (2011).

[6] T. Saastamoinen, T. Alasaarela, A. Lehmuskero, I. Vartiainen, N. Heikkilä, and M. Kuittinen, "Resonance waveguide reflectors with semi-wide bandwidth at the visible wavelengths," *Opt. Express* **19,** 2126–2132 (2011).

[7] R. Gumenyuk, I. Vartiainen, H. Tuovinen, S. Kivistö, Y. Chamorovskiy, and O. G. Okhotnikov, "Dispersion compensation technologies for femtosecond fiber system," *Appl. Opt.* **50,** 797–801 (2011).

[8] R. Gumenyuk, I. Vartiainen, H. Tuovinen, and O. G. Okhotnikov, "Dissipative dispersion-managed soliton 2μm thulium/holmium fiber laser," *Opt. Lett.* **36,** 609–611 (2011).

[9] Z. Ghadyani, I. Vartiainen, I. Harder, W. Iff, A. Berger, N. Lindlein, and M. Kuittinen, "Concentric ring metal grating for generating radially polarized light," *Appl. Opt.* **50,** 2451–2457 (2011).

[10] Y. Bourgin, I. Vartiainen, Y. Jourlin, M. Kuittinen, F. Celle, S. Tonchev, O. Parriaux, and T. Niemi, "Three-grating monolithic phase-mask for the single-order writing of large-period gratings," *J. Europ. Opt. Soc. Rap. Public.* **6,** 11016s (2011).

[11] B. Bai, X. Li, I. Vartiainen, A. Lehmuskero, G. Kang, J. Turunen, M. Kuittinen, and P. Vahimaa, "Anomalous complete opaqueness in a sparse array of gold nanoparticle chains," *Applied Physics Letters* **99,** 081911 (2011).

[12] I. Newton, *Opticks: or a Treatise of the Reflexion, Refractions, Inflexions an Colours* (Royal Society, London, 1904).

[13] T. Young, "The Bakerian Lecture: Experiments and Calculations Relative to Physical Optics," *Royal Society of London Philosophical Transactions Series I* **94,** 1–16 (1804).

[14] J. C. Maxwell, *A Treatise on Electricity and Magnetism,* Vol. 2, 3rd ed. (Dover Publications, New York, 1954).

[15] E. F. Schubert and K. J. Kyu, "Solid-state light sources getting smart," *Science* **308,** 1274–1278 (2005).

[16] P. W. Milonni and J. H. Eberly, *Laser Physics* (Wiley, Hoboken, NJ, 2010).

[17] M. J. Madou, *Fundamentals of Microfabrication : The Science of Miniaturization* (CRC Press, London, 2002).

[18] P. Rai-Choudhury, *Handbook of Microlithography, Micromachining, and Microfabrication* (SPIE Optical Engineering Press, London, 1997).

[19] Z. Cui, *Nanofabrication: Principles, Capabilities and Limits* (Springer, New York, 2010).

[20] J. Turunen and F. Wyrowski, *Diffractive Optics for Industrial and Commercial Applications* (Akademie Verlag, Germany, 1997).

[21] A. L. Schawlow and C. H. Townes, "Infrared and optical masers," *Phys. Rev.* **112,** 1940–1949 (1958).

[22] A. Javan, "Theory of a three-level maser," *Phys. Rev.* **107,** 1579–1589 (1957).

[23] T. H. Maiman, "Stimulated optical radiation in ruby," *Nature* **187,** 493–494 (1960).

[24] A. Kastler, "Quelques suggestions concernant la production optique et la détection optique d'une inégalité de population des niveaux de quantifigation spatiale des atomes. Application à l'expérience de Stern et Gerlach et à la résonance magnétique," *J. Phys. Radium* **11,** 255–265 (1950).

[25] F. Zernike, "The concept of degree of coherence and its application to optical problems," *Physica* **5,** 785–795 (1938).

[26] L. Mandel and E. Wolf, *Optical Coherence and Quantum Optics* (Cambridge University Press, Cambridge, 1995).

[27] J.-H. Lee, Y.-C. Ko, D.-H. Kong, J.-M. Kim, K. B. Lee, and D.-Y. Jeon, "Design and fabrication of scanning mirror for laser display," *Sensors and Actuators A: Physical* **96,** 223–230 (2002).

[28] B. G. Blundell, A. J. Schwarz, and D. K. Horrell, "Volumetric three-dimensional display systems: their past, present and future," *Engineering Science and Education Journal* **2,** 196–200 (1993).

[29] S. W. Henderson, P. J. M. Suni, C. P. Hale, S. M. Hannon, J. R. Magee, D. L. Bruns, and E. H. Yuen, "Coherent laser radar at 2 μm using solid-state lasers," *Geoscience and Remote Sensing, IEEE Transactions on* **31,** 4–15 (1993).

[30] M.-C. Amann, T. Bosch, M. Lescure, R. Myllylä, and M. Rioux, "Laser ranging: a critical review of usual techniques for distance measurement," *Opt. Eng.* **40,** 10–19 (2001).

[31] E. Wolf, "Unified theory of coherence and polarization of random electromagnetic beams," *Physics Letters A* **312,** 263 – 267 (2003).

[32] J. Tervo, T. Setälä, and A. T. Friberg, "Degree of coherence for electromagnetic fields," *Opt. Express* **11,** 1137–1143 (2003).

[33] T. Setälä, J. Tervo, and A. T. Friberg, "Contrasts of Stokes parameters in Young's interference experiment and electromagnetic degree of coherence," *Opt. Lett.* **31,** 2669–2671 (2006).

[34] J. Tervo, T. Setälä, and A. T. Friberg, "Theory of partially coherent electromagnetic fields in the space–frequency domain," *J. Opt. Soc. Am. A* **21,** 2205–2215 (2004).

[35] T. Setälä, J. Tervo, and A. T. Friberg, "Complete electromagnetic coherence in the space-frequency domain," *Opt. Lett.* **29,** 328–330 (2004).

[36] T. Setälä, J. Tervo, and A. T. Friberg, "Theorems on complete electromagnetic coherence in the space-time domain," *Optics Communications* **238,** 229–236 (2004).

[37] P. Réfrégier and F. Goudail, "Invariant degrees of coherence of partially polarized light," *Opt. Express* **13,** 6051–6060 (2005).

[38] A. Luis, "Overall degree of coherence for vectorial electromagnetic fields and the Wigner function," *J. Opt. Soc. Am. A* **24,** 2070–2074 (2007).

[39] D. Gabor, "Theory of communication," *J. Inst. Elect. Eng.* **93,** 429–457 (1946).

[40] R. Carminati and J.-J. Greffet, "Near-Field Effects in Spatial Coherence of Thermal Sources," *Phys. Rev. Lett.* **82,** 1660–1663 (1999).

[41] A. F. Fercher, C. K. Hitzenberger, M. Sticker, E. Moreno-Barriuso, R. Leitgeb, W. Drexler, and H. Sattmann, "A thermal light source technique for optical coherence tomography," *Optics Communications* **185,** 57–64 (2000).

[42] N. Wiener, "Generalized harmonic analysis," *Acta Mathematica* **55,** 117–258 (1930).

[43] A. Khintchine, "Korrelationstheorie der stationren stochastischen Prozesse," *Mathematische Annalen* **109,** 604–615 (1934).

[44] A. M. Yaglom, *An Introduction to Mathematical Stationary Random Functions* (Prentice-Hall, Englewood Cliffs, NJ, 1962).

[45] E. Wolf, "New theory of partial coherence in the space-frequency domain. Part I: spectra and cross spectra of steady-state sources," *J. Opt. Soc. Am.* **72,** 343–351 (1982).

[46] T. Setälä, J. Lindberg, K. Blomstedt, J. Tervo, and A. T. Friberg, "Coherent-mode representation of a statistically homogeneous and isotropic electromagnetic field in spherical volume," *Phys. Rev. E* **71,** 036618 (2005).

[47] A. Starikov and E. Wolf, "Coherent-mode representation of Gaussian Schell-model sources and of their radiation fields," *J. Opt. Soc. Am.* **72,** 923–928 (1982).

[48] R. C. Jones, "A New Calculus for the Treatment of Optical Systems," *J. Opt. Soc. Am.* **31,** 488–493 (1941).

[49] H. J. Hurwitz and R. C. Jones, "A New Calculus for the Treatment of Optical Systems," *J. Opt. Soc. Am.* **31,** 493–495 (1941).

[50] R. C. Jones, "New Calculus for the Treatment of Optical Systems. VIII. Electromagnetic Theory," *J. Opt. Soc. Am.* **46,** 126–131 (1956).

[51] G. G. Stokes, "On the composition and resolution of streams of polarized light from different sources," *Trans. Cambridge Philos. Soc.* **9,** 399–416 (1852).

[52] C. Brosseau, *Fundamentals of Polarized Light: A Statistical Optics Approach* (Wiley-Interscience, Englewood Cliffs, NJ, 1998).

[53] H. G. Berry, G. Gabrielse, and A. E. Livingston, "Measurement of the Stokes parameters of light," *Appl. Opt.* **16,** 3200–3205 (1977).

[54] F. Gori, "Measuring Stokes parameters by means of a polarization grating," *Opt. Lett.* **24,** 584–586 (1999).

[55] M. Born and E. Wolf, *Principles of Optics,* 7th ed. (Cambribge University press, 1997).

[56] R. Petit, *Electromagnetic Theory of Gratings* (Springer-Verlag, Germany, 1980).

[57] E. G. Loewen and E. Popov, *Diffraction Gratings and Applications* 1997).

[58] D. Rittenhouse, "An Optical Problem proposed by Mr. Hopkinson, and solved by Mr. Rittenhouse," *Trans. Amer. Phil. Soc.* **2,** 201 (1786).

[59] Z. Zhang and S. Satpathy, "Electromagnetic wave propagation in periodic structures: Bloch wave solution of Maxwell's equations," *Phys. Rev. Lett.* **65,** 2650–2653 (1990).

[60] H. P. Herzig, *Micro-optics: Elements, Systems and Applications* (Taylor & Francis, London, 1997).

[61] L. Li, "New formulation of the Fourier modal method for crossed surface-relief gratings," *J. Opt. Soc. Am. A* **14,** 2758–2767 (1997).

[62] L. Li, "Bremmer series, R-matrix propagation algorithm, and numerical modeling of diffraction gratings," *J. Opt. Soc. Am. A* **11,** 2829–2836 (1994).

[63] L. Li, "Formulation and comparison of two recursive matrix algorithms for modeling layered diffraction gratings," *J. Opt. Soc. Am. A* **13,** 1024–1035 (1996).

[64] L. Li, "Note on the S-matrix propagation algorithm," *J. Opt. Soc. Am. A* **20,** 655–660 (2003).

[65] P. Lalanne and G. M. Morris, "Highly improved convergence of the coupled-wave method for TM polarization," *J. Opt. Soc. Am. A* **13,** 779–784 (1996).

[66] E. Silberstein, P. Lalanne, J.-P. Hugonin, and Q. Cao, "Use of grating theories in integrated optics," *J. Opt. Soc. Am. A* **18,** 2865–2875 (2001).

[67] B. Bai and L. Li, "Group-theoretic approach to enhancing the Fourier modal method for crossed gratings with square symmetry," *J. Opt. Soc. Am. A* **23,** 572–580 (2006).

[68] L. Li, "Use of Fourier series in the analysis of discontinuous periodic structures," *J. Opt. Soc. Am. A* **13,** 1870–1876 (1996).

[69] R. W. Wood, "On a remarkable case of uneven distribution of light in a diffraction grating spectrum," *Phil. Mag.* **4,** 369–402 (1902).

[70] J. C. Harvey Palmer, "Parallel diffraction grating anomalies," *J. Opt. Soc. Am.* **42,** 269–273 (1952).

[71] A. Hessel and A. A. Oliner, "A new theory of Wood's anomalies on optical gratings," *Appl. Opt.* **4,** 1275–1297 (1965).

[72] L. Mashev and E. Popov, "Diffraction efficiency anomalies of multicoated dielectric gratings," *Optics Communications* **51,** 131–136 (1984).

[73] L. Mashev and E. Popov, "Zero order anomaly of dielectric coated gratings," *Optics Communications* **55,** 377–380 (1985).

[74] L. B. Stotts, "Eigenvalue expression for multilayer thin-film optical branch and mode resonant structures," *Optics Communications* **17,** 133–140 (1976).

[75] R. Magnusson and S. S. Wang, "New principle for optical filters," *Applied Physics Letters* **61,** 1022–1024 (1992).

[76] S. S. Wang and R. Magnusson, "Theory and applications of guided-mode resonance filters," *Appl. Opt.* **32,** 2606–2613 (1993).

[77] Z. S. Liu, S. Tibuleac, D. Shin, P. P. Young, and R. Magnusson, "High-efficiency guided-mode resonance filter," *Opt. Lett.* **23,** 1556–1558 (1998).

[78] Y. Ding and R. Magnusson, "Resonant leaky-mode spectral-band engineering and device applications," *Opt. Express* **12,** 5661–5674 (2004).

[79] F. Pigeon, O. Parriaux, Y. Ouerdane, and A. Tishchenko, "Polarizing grating mirror for CW Nd:YAG microchip lasers," *Photonics Technology Letters, IEEE* **12,** 648–650 (2000).

[80] T. Moser, H. Glur, V. Romano, F. Pigeon, O. Parriaux, M. A. Ahmed, and T. Graf, "Polarization-selective grating mirrors used in the generation of radial polarization," *Applied Physics B: Lasers and Optics* **80,** 707–713 (2005).

[81] K. Kneipp, H. Kneipp, I. Itzkan, R. R. Dasari, and M. S. Feld, "Ultrasensitive chemical analysis by Raman spectroscopy," *Chemical Reviews* **99,** 2957–2976 (1999).

[82] A. Campion and P. Kambhampati, "Surface-enhanced Raman scattering," *Chem. Soc. Rev.* **27,** 241–250 (1998).

[83] N. Ganesh, I. D. Block, P. C. Mathias, W. Zhang, E. Chow, V. Malyarchuk, and B. T. Cunningham, "Leaky-mode assisted

fluorescence extraction: application to fluorescence enhancement biosensors," *Opt. Express* **16,** 21626–21640 (2008).

[84] A. Mizutani, H. Kikuta, and K. Iwata, "Wave localization of doubly periodic guided-mode resonant grating filters," *Optical Review* **10,** 13–18 (2003).

[85] R. C. McPhedran, L. C. Botten, M. S. Craig, M. Nevière, and D. Maystre, "Lossy Lamellar Gratings in the Quasistatic Limit," *Optica Acta* **29,** 289–312 (1982).

[86] D. C. Flanders, "Submicrometer periodicity gratings as artificial anisotropic dielectrics," *Applied Physics Letters* **42,** 492 –494 (1983).

[87] C. W. Haggans, L. Li, and R. K. Kostuk, "Effective-medium theory of zeroth-order lamellar gratings in conical mountings," *J. Opt. Soc. Am. A* **10,** 2217–2225 (1993).

[88] G. R. Bird and J. Maxfield Parrish, "The wire grid as a near-infrared polarizer," *J. Opt. Soc. Am.* **50,** 886–891 (1960).

[89] E. Hecht and A. Zajac, *Optics* (Addison-Wesley, Reading, MA, 1974).

[90] M. Honkanen, V. Kettunen, M. Kuittinen, J. Lautanen, J. Turunen, B. Schnabel, and F. Wyrowski, "Inverse metal-stripe polarizers," *Applied Physics B: Lasers and Optics* **68,** 81–85 (1999).

[91] J. Tervo and J. Turunen, "Paraxial-domain diffractive elements with 100% efficiency based on polarization gratings," *Opt. Lett.* **25,** 785–786 (2000).

[92] T. Ito and S. Okazaki, "Pushing the limits of lithography," *Nature* **406,** 1027–1031 (2000).

[93] U. D. Zeitner and E.-B. Kley, "Advanced lithography for micro-optics," in *Society of Photo-Optical Instrumentation En-*

gineers (SPIE) Conference Series, Vol. 6290, Society of Photo-Optical Instrumentation Engineers (SPIE) Conference Series (2006).

[94] A. Hohenau, H. Ditlbacher, B. Lamprecht, J. R. Krenn, A. Leitner, and F. R. Aussenegg, "Electron beam lithography, a helpful tool for nanooptics," *Microelectronic Engineering* **83,** 1464–1467 (2006), Micro- and Nano-Engineering MNE 2005.

[95] L. J. Guo, "Nanoimprint Lithography: Methods and Material Requirements," *Advanced Materials* **19,** 495–513 (2007).

[96] I. Haller, M. Hatzakis, and R. Srinivasan, "High-resolution positive resists for electron-beam exposure," *IBM Journal of Research and Development* **12,** 251–256 (1968).

[97] C. Vieu, F. Carcenac, A. Ppin, Y. Chen, M. Mejias, A. Lebib, L. Manin-Ferlazzo, L. Couraud, and H. Launois, "Electron beam lithography: resolution limits and applications," *Applied Surface Science* **164,** 111–117 (2000).

[98] G. S. Oehrlein, "Reactive-ion etching," *Physics Today* **39,** 26–33 (1986).

[99] T. K. S. Wong and S. G. Ingram, "Fabrication of sub-20 nm trenches in silicon nitride using CHF_3/O_2 reactive ion etching and oblique metallization," *Journal of Vacuum Science Technology B: Microelectronics and Nanometer Structures* **10,** 2393–2397 (1992).

[100] B. E. E. Kastenmeier, P. J. Matsuo, J. J. Beulens, and G. S. Oehrlein, "Chemical dry etching of silicon nitride and silicon dioxide using CF4/O2/N2 gas mixtures," *Journal of Vacuum Science Technology A: Vacuum, Surfaces, and Films* **14,** 2802–2813 (1996).

[101] J. E. Mahan, *Physical vapor deposition of thin films* (Wiley, New York, NY, 2000).

[102] S. Nakada, M. Yamaguchi, M. Yamamoto, and H. Ishimaru, "Electron beam evaporator constructed from aluminum alloy and the gettering effect of chromium films," *Journal of Vacuum Science Technology A: Vacuum, Surfaces, and Films* **12,** 1631–1634 (1994).

[103] J. E. Simpkins and P. Mioduszewski, "Summary abstract: Comparison of Ti and Cr gettering," *Journal of Vacuum Science and Technology* **20,** 1321 (1982).

[104] J. J. Wang, L. Chen, X. Liu, P. Sciortino, F. Liu, F. Walters, and X. Deng, "30-nm-wide aluminum nanowire grid for ultrahigh contrast and transmittance polarizers made by UV-nanoimprint lithography," *Applied Physics Letters* **89,** 141105–141105–3 (2006).

[105] F. Engelmark, G. F. Iriarte, and I. V. Katardjiev, "Selective etching of Al/AlN structures for metallization of surface acoustic wave devices," *Journal of Vacuum Science Technology B: Microelectronics and Nanometer Structures* **20,** 843–848 (2002).

[106] E. Hutter and J. H. Fendler, "Exploitation of Localized Surface Plasmon Resonance," *Advanced Materials* **16,** 1685–1706 (2004).

[107] U. Kreibig, *Optical Properties of Metal Clusters* (Springer-Verlag, Berlin, Germany, 1995).

[108] T. Weber, T. Käsebier, E.-B. Kley, and A. Tünnermann, "Broadband iridium wire grid polarizer for UV applications," *Opt. Lett.* **36,** 445–447 (2011).

[109] M. Ritala, K. Kukli, A. Rahtu, P. I. Räisänen, M. Leskelä, T. Sajavaara, and J. Keinonen, "Atomic Layer Deposition of Oxide Thin Films with Metal Alkoxides as Oxygen Sources," *Science* **288,** 319–321 (2000).

[110] M. Ritala and J. Niinistö, "Chapter 4 Atomic Layer Deposition," in *Chemical Vapour Deposition: Precursors, Processes and*

Applications (The Royal Society of Chemistry, 2009), pp. 158–206.

[111] J. A. Hoffnagle, W. D. Hinsberg, M. Sanchez, and F. A. Houle, "Liquid immersion deep-ultraviolet interferometric lithography," *Journal of Vacuum Science Technology B: Microelectronics and Nanometer Structures* **17,** 3306–3309 (1999).

[112] A. J. Haes and R. P. Van Duyne, "A Nanoscale optical biosensor: sensitivity and selectivity of an approach based on the localized surface plasmon resonance spectroscopy of triangular silver nanoparticles," *Journal of the American Chemical Society* **124,** 10596–10604 (2002).

Ismo Vartiainen

Polarization control and coherence–polarization mixing by sub-wavelength gratings

This thesis considers polarization control by means of sub-wavelength gratings. The thesis investigates inverse polarization effect in surface-relief gratings. The design and fabrication of these structures is discussed. Furthermore, experimental results for polarization gratings for lossless beam splitting and for measurement of Stokes parameters are described. In addition, this thesis gives insight for new optical phenomenon called coherence-polarization mixing, in which partial correlation of the polarization components is transferred to partial polarization.

UNIVERSITY OF
EASTERN FINLAND

Publications of the University of Eastern Finland
Dissertations in Forestry and Natural Sciences

ISBN 978-952-61-0619-9
ISSN 1798-5668